出國報告（出國類別：參加國際會議）

參加第20屆傳輸現象研討會

服務機關：海軍軍官學校
姓名職稱：葉豐賓 教授
派赴國家：加拿大
報告日期：98 年8 月12 日
出國期間：98 年7 月3 日至98 年7 月12 日

摘要

第 20 屆傳輸現象研討會於 2009 年 7 月 7 日至 2009 年 7 月 10 日於加拿大維多利亞市中心的Delta Victoria Ocean Pointe Resort and Spa舉行。該研討會吸引上百位來自世界各地之專家學者與會，發表了上百場專題演講與壁報論文展示。內容範圍從基礎科學到應用工程系統、熱流體工程之傳輸現象，包括以下幾個方面：熱傳質傳、先進及替代能源系統、實驗/計算流體動力學、燃料電池、燃燒反應流、碳捕獲及封存、化工過程系統、電子設備冷卻、能量轉換、工業空氣動力學及風力工程、微型和納米尺度傳輸、熱交換器、紊流與流動穩定性、熱流體機械、多孔介質中之傳輸、熱核反應器、多相系統的傳輸現象、製造和材料加工、環境系統、可視化/影像、生物工程與生物熱流體動力學、燃氣渦輪機熱傳等。藉由參加多場學術演講與壁報觀摩，吸收新知，瞭解國際間目前在基礎科學、應用工程、熱流體工程之傳輸現象之研究趨勢與方向，獲益良多。

目次

摘要……2
參加會議目的……4
參加會議過程……4
與會心得……6
建議……6
附錄……7

參加會議目的

ISTP 屬於多學科的國際會議，此會議提供了來自世界各地的研究人員、科學家和從業者交流信息的一個論壇，不僅提出新的信息，並討論未來重點領域的傳輸現象方向。傳輸現象包括流動的液體、熱傳質傳、電力、中子和粒子等。ISTP 研討會已舉辦了 19 屆，歷年舉行的地點如下：Honolulu 1985, Tokyo 1987, Taipei 1988, Sydney 1991, Beijing 1992, Seoul 1993, Acapulco 1994, San Francisco 1995, Singapore 1996, Kyoto 1997, Taipei 1998, Istanbul 2000 , Victoria 2002, Bali 2003, Bangkok 2004, Prague 2005, Toyama 2006, Daejeon 2007 and Reykjavik 2008。今年第 20 屆研討會則由加拿大維多利亞大學能源整合系統協會所舉辦。藉由參加多場學術演講與壁報觀摩，吸收新知，瞭解國際間目前在基礎科學、應用工程、熱流體工程之傳輸現象之研究趨勢與方向。

參加會議過程

第 20 屆傳輸現象研討會於 2009 年 7 月 7 日至 2009 年 7 月 10 日於加拿大維多利亞市中心的Delta Victoria Ocean Pointe Resort and Spa舉行。該研討會吸引上百位來自世界各地之專家學者與會，發表上百場專題演講與壁報論文展示。內容範圍從基礎科學到應用工程系統、熱流體工程之傳輸現象。

本大會之專題演講共分爲 5 個演講廳(ASCOT、BALFOUR、CHELSEA/DERBY、SONGHEES SUITE、HARBOUR ROOM)同時舉行，

區分 16 大主題，每大主題又區分爲數個場次，在不同時段於不同演講廳進行演講。共 39 場次，發表 159 篇論文。

(1) Heat and MassTransfer (9);

(2) Micro- and Nano-scale Transport (4);

(3) Experimental and Computational Fluid Dynamics (6) ;

(4) Transport in Porous Media (2);

(5) Transport in Porous Media (2) ;

(6) Combustion and Reacting Flows (2)

(7) Transport Phenomena in Multi-Phase Systems (3)

(8) Turbulence and Flow Instabilities (2)

(9) Bioengineering and Biothermal Fluid Dynamics (2)

(10) Transport in Porous Media / Fuel Cells

(11) Heat Exchangers

(12) Electronic Equipment Cooling

(13) Transport Phenomena – General

(14) Environ. Systems / Manuf. And Materials Processing

(15) Visualization/Imaging Techniques

(16) Advanced Alternative Energy Sys. / Chem. Proc. Systems

主辦單位將此國際會議之專題演講區設立於Delta Victoria Ocean Pointe Resort and Spa，而壁報論文展示區則設立於 University Club, Univ. of Victoria。研討會的開幕式特別邀請 Simon Fraser 大學的 Michael Eikerling 博士做專題演講，講題爲：**“The Story of Water in PEM Fuel Cells”** 。Eikerling 博士是理論化學物理和電化學專家。 研究領域主要結合了頻譜的理論方法和分子模擬方法，分析多尺度電化學能量轉換過程中之傳輸現象以及其與材料的結構、性質、性能與設備的關係。Eikerling 博士參與西門菲沙(Simon Fraser)大學和美國國家研究委員會研究所燃料電池創新(IFCI)

之研究。研究工作結合了基本理論的發展與燃料電池中聚合物電解質性能最佳化的應用研究。 他的貢獻包括引用液壓滲透模型於水傳輸燃料電池膜和催化層運作的基礎結構物理模型。他還首先利用量子力學的計算，以說明聚合物與水界面間的電化學和傳輸現象。他的研究工作提升了先進燃料電池元件和材料的設計。Eikerling 博士已在代表性期刊發表了 36 篇相關之論文，包括三篇專題文章，並且是 7 本書籍的共同作者。在過去六年中，受邀擔任 40 多個場次之演講。Eikerling 博士是好幾個學術團體的會員，在 NRC-IFCI，他負責的研究項目是以理化理論和分子模式模擬燃料電池中聚合物電解質的材料和傳輸過程，並且負責協調加拿大和德國之間以及 NRC 和 CEA 之間燃料電池的合作研究項目。

與會心得

本會議爲國際研究傳輸現象極爲知名且重要之研討會，目前已舉辦第 20 屆，會議中共發表數百篇之論文。藉由參加多場學術演講與壁報論文觀摩，吸收新知，瞭解國際間目前在基礎科學、應用工程、熱流體工程之傳輸現象之研究趨勢與方向，獲益良多。

建議

應多鼓勵大專院校之師生多參與類似之國際學術活動，以增進學校於國際之能見度。

附錄

A SEMI-ANALYTICAL MODEL TO STUDY THE STATIC CHARACTERISTICS OF THE PLASMA SHEATH

F. B. Yeh

Department of Marine Mechanical Engineering
ROC Naval Academy, Taiwan, R. O. C.

ABSTRACT

The characteristics of sheath dominate the ions and electrons flux transport from plasma to a negative bias surface. Based on the kinetic analysis, some analytical expressions are given for the spatial variations of density and fluid speed of ion and electron, potential and electric field in the sheath for arbitrary negative bias voltage at the wall. The predicted spatial variation of the electric field in the sheath is found to agree well with experimental data. The effects of dimensionless bias voltage, ion source strength, reflectivities of the ion and electron on the wall, ion-electron mass ratio, charge number, and electron-ion source temperature ratio at the presheath edge on the density and fluid speed of ion and electron, the potential and electric field in the sheath are obtained in this work.

INTRODUCTION

The potential gradient, i.e., electric field, can play a strong role in the transport of impurity ions in the plasma. In fusion devices, the impurity ions release from the wall surface by ion sputtering can be controlled to return to a limiter or divertor plate while the electric field intensity in the sheath is higher. In contrast, the electric field is weak then the impurities could easily move back into the bulk plasma. Hence, the potential and electric field profiles in the sheath are very important to investigate the energy and momentum flux of the ions and electrons striking the wall surface.

In many applications, the electrical characteristics of bounded plasma–sheath systems are determined by the behavior of the sheath. It, therefore, becomes important to find the relationship between the sheath characteristics and the plasma parameters. Many papers have been published to treat plasma-wall system, including the theoretical [1-6] and experimental [7-9] works in evaluating the effects of physical processes on the potential variation in the presheath and sheath. In the theoretical models, one method is to find numerical solution of plasma balance equation from the center of the plasma to the wall simultaneously. The other is to consider models for plasma and for sheath, solve them separately and join them together. To optimize the quality of plasma processing, a bias voltage is often applied to the substrate, which controls the kinetic energy of the impinging ion flux.

Since plasma particle and heat flux to a solid surface are controlled by sheath electrical field, we wishes to predict these foregoing quantities as a function of electron and ion source temperatures, ion and electron reflectivities, ion charge number, ion mass, applied negative bias voltage, etc. In this work, the plasma parameters affect the density and fluid speed of the ion and electron, potential and electric field distributions in the sheath can be determined.

KINETIC MODEL AND ANALYSIS

In this work, a plasma composed of a presheath and sheath is in contact with a wall with electrically negative bias voltage partially reflecting and secondarily emitting ions and electrons. The major assumptions made are same as our previous works [2, 3].

Asymptotic Analysis - Presheath

The dimensional poisson's equation applying in the presheath and sheath is

$$-\varepsilon_0 \frac{d^2\phi}{dx^2} = e(Z_i n_i - n_e) \tag{1}$$

The dimensionless form of equation (1) in the presheath can be expressed as

$$\varepsilon^2 \frac{d^2\chi}{d\eta^2} = Z_i n_i^* - n_e^* \tag{2}$$

The dimensionless quantities are defined as

$$\chi = -\frac{e\phi}{K_B T_{e0}},\ \eta = \frac{x}{L},\ \varepsilon = \frac{\lambda_D}{L},$$
$$n_i^* = \frac{n_i}{n_{e0}},\ n_e^* = \frac{n_e}{n_{e0}} \tag{3}$$

where ε is the ratio of the Debye length λ_D to the characteristic extension L of the plasma. L and λ_D are the characteristic lengths in the presheath and sheath, respectively. The latter is defined as $\lambda_D = (\varepsilon_0 k_B T_{e0} / n_{e0} e^2)^{1/2}$. On the presheath scale the sheath thickness is infinitely thin. The left-hand side of equation (2) approaches to zero and is neglected that results in $Z_i n_i^* = n_e^*$. Hence, the plasma in the presheath is quasineutral. The dimensionless electric field distribution function in the presheath can be expressed as [2]

$$E_p^* = \frac{d\chi}{d\eta} = \pi A S_i h(\chi)\left[\frac{\sqrt{\chi}}{1 - 2\sqrt{\chi} D(\sqrt{\chi})}\right] \tag{4}$$

with

$$A = \frac{Z_i^{\frac{3}{2}} \kappa(1+\rho)}{(1-\rho)(Z_i\kappa + 1)}, S_i = \frac{S_0 L}{n_{e0}} \sqrt{\frac{m_i}{2K_B T_{e0}}} \tag{5}$$

The variable of $h(\chi)$ denotes the spatially nonuniform source strength. The sheath edge potential χ_b can be determined in [2].

$$\frac{2}{\sqrt{\pi Z_i \kappa}} D(\sqrt{\chi_b}) = e^{Z_i \kappa \chi_b} \operatorname{erfc}(\sqrt{Z_i \kappa \chi_b}) \tag{6}$$

The Dawson and complementary error functions are, respectively, defined in [3]. The dimensionless electric field in the presheath is defined as $E_p^* = E_p / (k_B T_{e0} / eL)$. The assumption of that the source is uniform in the bulk plasma $h(\chi) = 1$ [4], integrating equation (4) and invoking the boundary condition $\eta = 0$, $\chi = 0$, the spatial variation of dimensionless potential distribution in the presheath is expressed as

$$\eta = \frac{2D(\sqrt{\chi})}{\pi A S_i} \tag{7}$$

Asymptotic Analysis - Sheath

The magnitude of sheath width is a few electron debye lengths in the sheath. The dimensionless coordinate is redefined as $\xi = (x - x_r)/\lambda_D = (\eta - \eta_r)/\varepsilon$ to solve the sheath. Here, x_r designates an arbitrary reference point defining the origin of the sheath space coordinate ξ. On this sheath scale the presheath is infinitely remote. Hence, the dimensionless poisson's equation in the sheath is

$$\frac{d^2\chi}{d\xi^2} = Z_i n_i^* - n_e^* \tag{8}$$

Equation (8) can be expressed further as

$$\left(\frac{d\chi}{d\xi}\right)^2 = \varepsilon^2 {E_{p,b}^*}^2 + 2(M_{ftot}^* - M_{ftotb}^*) \tag{9}$$

where M_{ftot}^* and M_{ftotb}^* represent the sum of the momentum flux of the ions and the electrons at the evaluating point and the sheath edge, respectively, and which are define as [10]

$$M_{ftot}^* = n_i^* {u_i^*}^2 + p_i^* - \tau_i^* + \frac{n_e^* {u_e^*}^2}{M} + p_e^* - \tau_e^* \tag{10}$$

$$M_{ftotb}^* = \frac{n_{ib}^* \Omega_{2b}}{\kappa} + e^{-\chi_b} + \frac{\rho_e - 1}{2} \times \left[e^{-\chi_b} \operatorname{erfc}(\sqrt{\chi_w - \chi_b}) + 2\sqrt{\frac{\chi_w - \chi_b}{\pi}} e^{-\chi_w}\right] \tag{11}$$

With

$$n_i^* = \frac{1}{Z_i}\{\Xi_2(\chi) + e^{Z_i\kappa\chi}\mathrm{erfc}[\sqrt{Z_i\kappa(\chi-\chi_b)}] - \Xi_1(\chi)\} \quad (12)$$

$$u_i^* = \frac{1}{n_i^* Z_i} e^{-\chi_b}\Omega_{1b} \quad (13)$$

$$n_e^* = e^{-\chi}[1 + \frac{\rho_e - 1}{2}\mathrm{erfc}(\sqrt{\chi_w - \chi})] \quad (14)$$

$$u_e^* = \frac{(1-\rho_e)}{n_e^*}\sqrt{\frac{M}{2\pi}}e^{-\chi_w} \quad (15)$$

The functions Ω_{1b}, Ω_{2b}, $\Xi_1(\chi)$ and $\Xi_2(\chi)$ are defined in our previous work [3]. The dimensionless momentum flux is defined as $M_f^* = M_f / n_{eo}k_B T_{e0}$. The dimensionless ion and electron fluid speed are defined as $u^* = u/(k_B T_{e0}/m_i)^{1/2}$. The transport variables of dimensionless ion and electron mean pressure p^* and fluid-like viscous stress τ^* are defined in [3]. The wall potential is defined as $\chi_w = \chi_{bias} + \chi_f$, χ_{bias} and χ_f denote the dimensionless applied negative bias voltage and the floating potential at the wall, respectively. The latter is defined as [10]

$$\chi_f = \chi_b + \ln(\frac{1-\rho_e}{\Omega_{1b}}\sqrt{\frac{M}{2\pi}}) \quad (16)$$

The dimensional electrical field is continuous across the sheath edge, the dimensionless electric field at the sheath edge at the sheath side is defined as $E_{s,b}^* = \varepsilon E_{p,b}^*$. E_s^* is the dimensionless electric field in the sheath and is defined as $E_s^* = E_s/(k_B T_{e0}/e\lambda_D)$. The dimensionless electric field at the sheath edge at the presheath side is defined as $E_{p,b}^* = d\chi/d\eta|_{\eta=\eta_b}$ which can be evaluated from equation (4). The dimensionless electric field distribution in the sheath is

$$E_s^* = \frac{d\chi}{d\xi} = \sqrt{\varepsilon^2 {E_{p,b}^*}^2 + 2(M_{ftot}^* - M_{ftotb}^*)} \quad (17)$$

Integrating equation (17), the spatial variation of the dimensionless potential distribution in the sheath is

$$\xi - \xi_w = \int_{\chi_w}^{\chi} \frac{d\chi'}{\sqrt{\varepsilon^2 {E_{p,b}^*}^2 + 2(M_{ftot}^* - M_{ftotb}^*)}} \quad (18)$$

RESULTS AND DISCUSSION

To confirm relevancy and accuracy of this model, the spatial distribution of predicted electric field in the sheath between a helium plasma and brass workpiece is compared with experimental data provided by Watanabe et al. [8], as shown in Fig. 1.

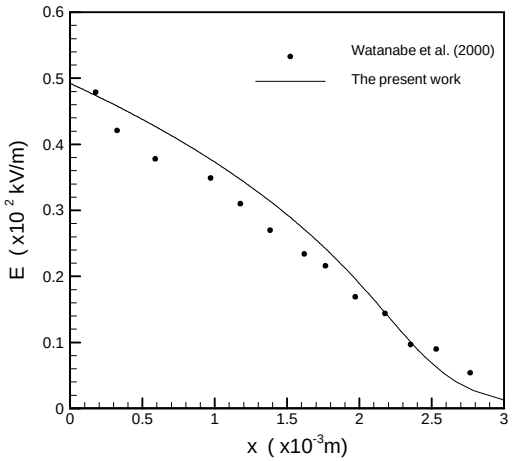

Figure1. A comparison between the predicted electric field distribution and experimental results in the sheath [8].

The different ε affecting the dimensionless potential and electric field, density and fluid speed of ion and electron profiles in the sheath as shown in Fig. 2(a) to 2(c), respectively. The absolute value of abscissa, $|\xi - \xi_w|$, represents the distance from the wall surface. The solid line (and following figures) is the predicted result based on the dimensionless reference parameters from Table 1. The dimensionless potential and electric field rapid increase

monotonically from the sheath edge ($|\xi-\xi_w|$ = 13.3) to the wall surface ($|\xi-\xi_w|$ = 0). The characteristics of the presheath, and the sheath edge and wall potentials are independent of the ε. For $\varepsilon=1$, the dimensionless electric field at the sheath edge at the sheath side is identical to that at the preshesth side. The corresponding electric field at the sheath edge is around $E^*_{s,b}=2\times10^{-1}$. A decrease in ε results in decreasing the dimensionless electric field at the sheath edge at the sheath side. The electric field at the sheath edge is around $E^*_{s,b}=2\times10^{-4}$ for $\varepsilon=1\times10^{-3}$.

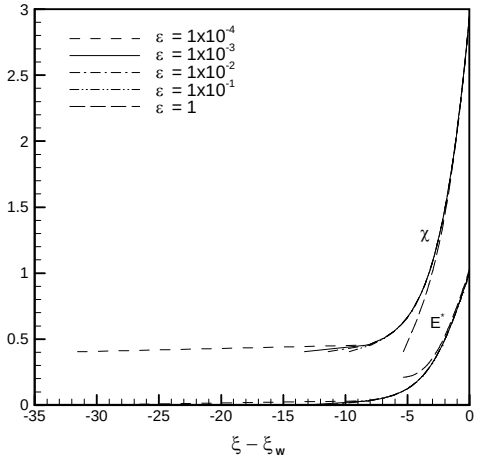

2(a)

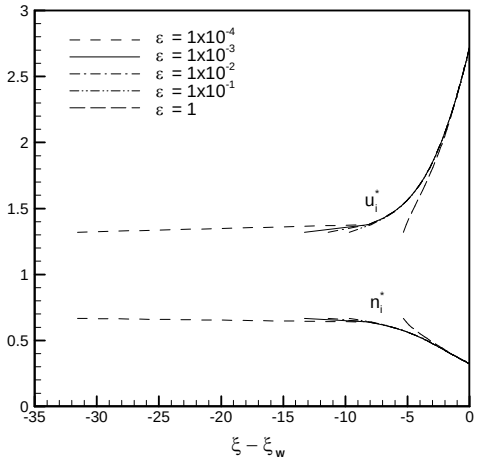

2(b)

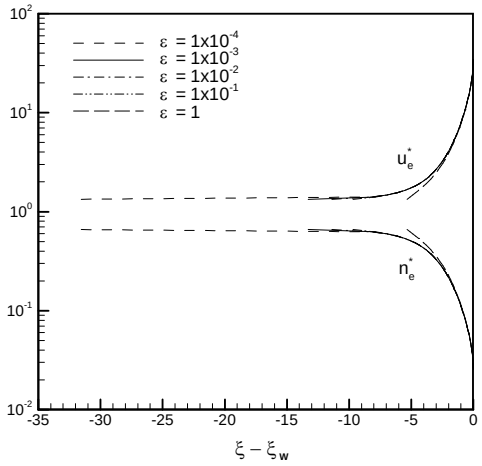

2(c)

Figure 2. Spatial variations of dimensionless (a) potential and electric field, (b) ion and (c) electron density and fluid speed in the sheath for different ε.

Table 1 Values of the dimensionless reference parameters

$\rho=0$	$\rho_e=0$	$M=1836$	$Z_i=1$
$\kappa=1$	$S_i=0.5$	$\chi_{bias}=0$	$\varepsilon=1\times10^{-3}$

The dimensionless electric field at the sheath edge at the sheath side approaches zero for $\varepsilon\approx0$. As shown in Fig. 2(b) and 2(c), the dimensionless ion and electron densities decrease and fluid speed increase in the direction toward the wall surface for $\varepsilon=1\times10^{-3}$. The density and fluid speed of the ion and electron at the sheath edge and wall are constants for different ε. It can be observed in figures 2(a) to 2(c) that the different ε has little effect on the spatial variations of the potential, electric field, density and fluid speed of ion and electron in the sheath near the wall.

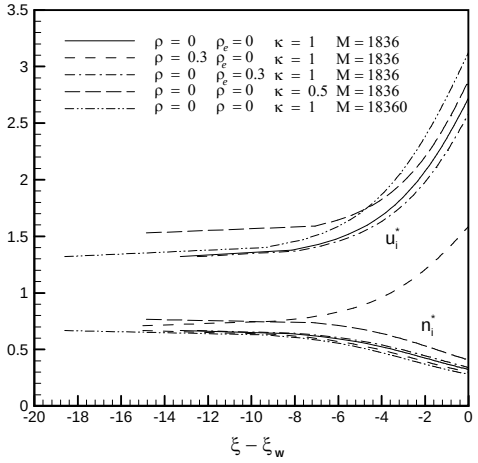

3(a)

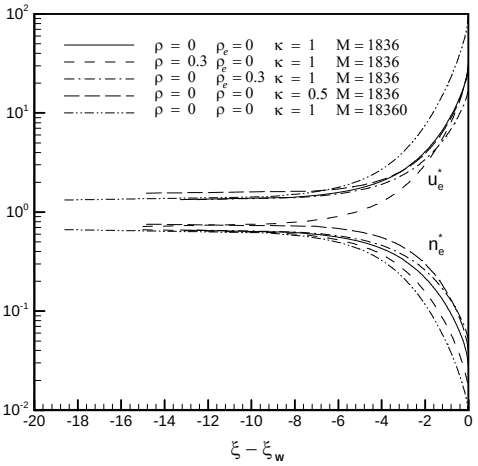

3(b)

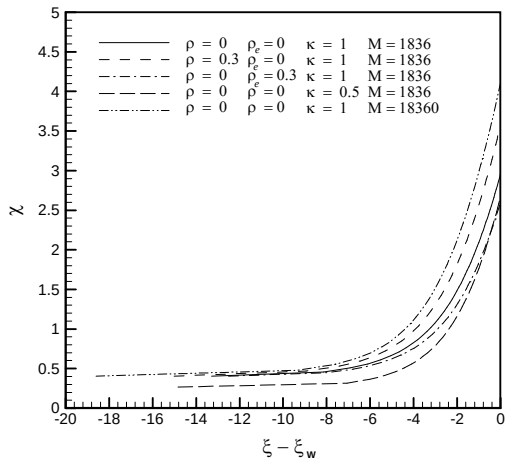

3(c)

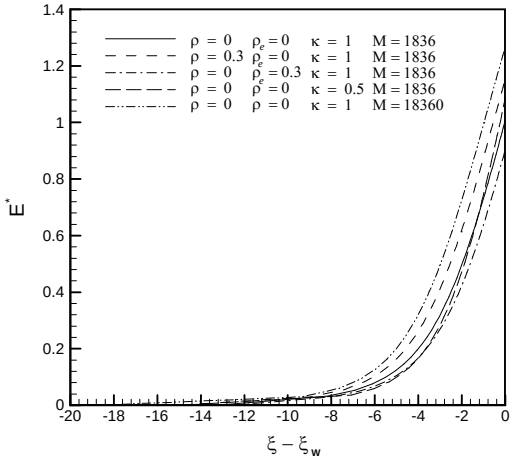

3(d)

Figure 3. Spatial variations of dimensionless (a) ion and (b) electron density and fluid speed, (c) potential and (d) electric field in the sheath for different ion and electron reflectivities, electron-ion source temperature ratio at presheath edge and ion-electron mass ratio.

Dimensionless spatial variations of density and fluid speed of ion and electron, potential and electric field in the sheath for different ion and electron reflectivities, electron-ion source temperature ratio at presheath edge and ion-electron mass ratio are shown in Figs. 3(a) to 3(d), respectively. An increase in ion reflectivity reducesthe ion fluid speed and current density at the sheath edge that results in increasing the wall potential [as shown in Fig. 3(c)] to reduce the electron current density at the wall [3]. Hence, an increase in ion reflectivity decreases the density and fluid speed of ion and electron in the sheath as shown in Figs. 3(a) and 3(b), respectively. The sheath edge potential is Independent of the ion reflectivity. An increase in ion reflectivity increases the electric field at the sheath edge and the increment of momentum flux across the sheath [10] that result in increasing the electric field at the wall [as shown in Fig. 3(d)]. A decrease in electron-ion source temperature ratio represents an increase in ionization rate that results in increasing the ion current density at the sheath edge and decreasing the sheath edge and wall potentials [3]. This leads to increase the density and fluid speed of ion and electron in the sheath. The electric field at the

sheath edge decrease with decreasing the electron-ion source temperature ratio at the presheath edge but the increment of momentum flux across the sheath increases [10]. However, the electric field at the wall increases with decreasing the electron- ion source temperature ratio. The characteristics of the presheath are independent of the electron reflectivity and ion-electron mass ratio. Because that the ion current density at the sheath edge is constant for different electron reflectivity, an increase in electron reflectivity results in decreasing the wall potential to increase electron current density at the wall [3]. An increase in electron reflectivity increases density of ion and electron but decreases fluid speed of ion and electron. The increment of momentum flux across the sheath decreases with increasing the electron reflectivity [10]. Hence, the electric field at the wall decreases with increasing the electron reflectivity. An increase in ion-electron mass ratio represents an increase in electron current density at the wall that results in increasing the wall potential to reduce electron current density [3]. An increase in ion-electron mass ratio decreases density of ion and electron but increases fluid speed of ion and electron. The increment of momentum flux across the sheath increases with increasing the ion-electron mass ratio [10] that results in the electric field at the wall increases.

Different charge number, ion source strength and bias voltage affecting the dimensionless spatial variations of density and fluid speed of ion and electron, potential and electric filed in the sheath are shown in Figs. 4(a) to 4(d), respectively. An increase in charge number represents an increase in ion current density at the sheath edge that result in increasing the sheath edge potential and decreasing the wall potential to reduce ion current density at the wall [3]. Hence, the density of ion and electron decrease and the fluid speed of ion and electron increase. An increase in charge number results in increasing the electric fields at

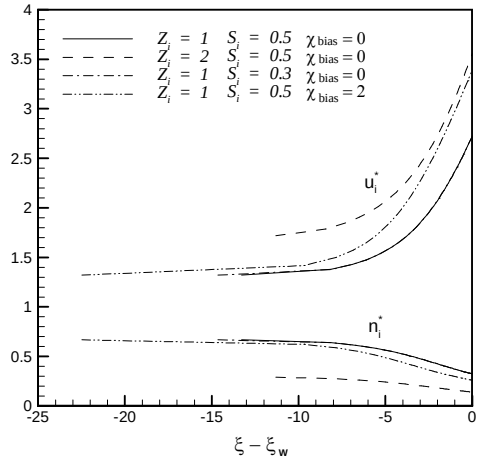

4(a)

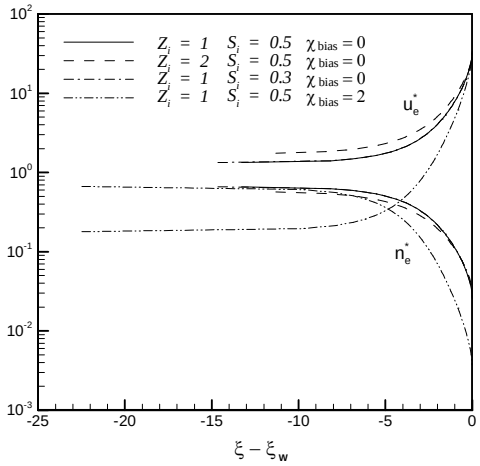

4(b)

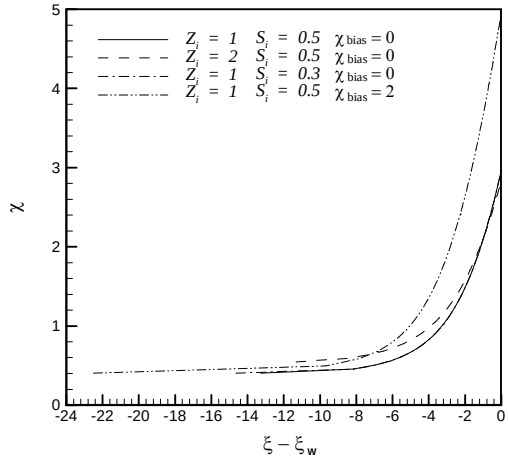

4(c)

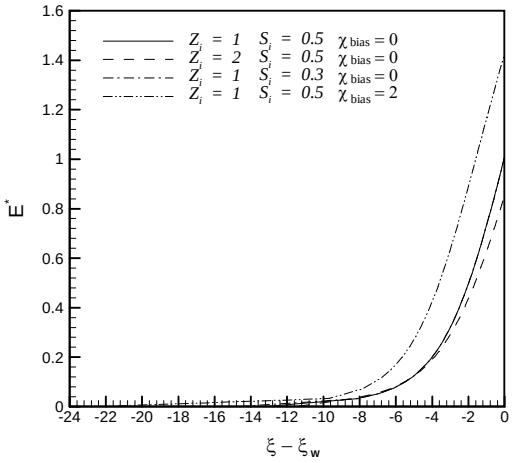

4(d)

Figure 4. Spatial variations of dimensionless (a) ion and (b) electron density and fluid speed, (c) potential and (d) electric field in the sheath for different charge number, ion source strength and bias voltage.

the sheath edge, and decreasing the electric fields at the wall and the increment of momentum flux across the sheath [10]. The sheathe edge and wall potential are independent of ion source strength. Hence, the variation of ion source strength has no effect on the potential, electric field, density and fluid speed of ion and electron profiles in the sheath. $\chi_{bias} = 0$ and $\chi_{bias} = 2$ represent the wall surface at the floating potential and applied negative bias potential, respectively. The characteristic of the presheath are independent of bias voltage but the effects of bias voltage on the characteristic of sheath are very large. An increase in bias voltage increases the ion fluid speed and decreases the ion density. The density and fluid speed of electron decrease with increasing the bias voltage. The increment of momentum flux across the sheath increases with the bias voltage [10] that results in the electric field at the wall increases.

CONCLUSIONS

The potential and electric field distributions in the sheath can be found in this work. Impurity ions release from the wall surface by ion sputtering can be controlled to return to the wall surface by using the higher electric field intensity in the sheath. The electric field intensities at the sheath edge and wall increase with increasing the ion reflectivity. Decrease the electron-ion source temperature ratio at the presheath edge and charge number result in increasing the electric field at the wall and decreasing the electric field at the sheath edge. An increase in the ion-electron mass ratio and bias voltage, and a decrease in the electron reflectivity result in increasing the electric field intensity at the wall.

NOMENCLATURE

e electron charge.

k_B Boltzmann constant.

M ion-electron mass ratio defined as m_i / m_e.

m_i ion mass.

n_{e0} electron density at the presheath edge.

S_0 ion average source strength.

S_i dimensionless ion average source strength.

T_{i0} ion ionization temperature at the presheath edge.

T_{e0} electron temperature at the presheath edge.

Z_i ion charge number.

ε_0 permittivity of free space.

ϕ potential.

ρ ion reflectivity.

ρ_e electron reflectivity.

κ electron-ion source temperature ratio at the presheath edge defined as T_{e0} / T_{i0}.

REFERENCES

1.Self, S. A. (1965): "Asymptotic plasma and sheath representations for low-pressure discharges". *Journal of Applied Physics*, Vol.36, pp. 456-459.

2.Wei, P. S., Yeh, F. B. and Ho, C. Y. (2000): "Distribution Functions of Positive Ions and Electrons in a Plasma Near a Surface". *IEEE Transactions on Plasma Science*, Vol. 28, pp. 1244-1253.

3.Wei, P. S. and Yeh, F. B. (2000): "Fluid-Like Transport Variables in a Kinetic, Collisionless Plasma Near a Surface with Ion and Electron Reflection". *IEEE Transactions on Plasma Science*, Vol. 28, pp. 1233-1243.

4.Emmert, G. A., Wieland, R. M., Mense, A. T. and Davidson, J. N. (1980): "Electric sheath and presheath in a collisionless, finite ion

temperature plasma". *Physics of Fluids,* Vol. 23, pp. 803-812.
5.Riemann, K. –U. (2006): "Plasma-sheath transition in the kinetic Tonks-Langmuir model". *Physics of Plasmas,* Vol. 13, pp. 063508-1-063508-13.
6.Sternberg, N. and Godyak, V. (2003): "Patching Collisionless Plasma and Sheath Solutions to Approximate the Plasma-Wall Problem". *IEEE Transactions on Plasma Science,* Vol. 31, pp.1395-1401.
7.Goeckner, M. J., Goree, J. and Sheridan, T. E. (1992): "Measurements of ion velocity and density in the plasma sheath". *Physics.of Fluids B,* Vol.4, pp.1663-1670.
8.Watanabe, M., Takiyama, K. and Oda, T. (2000): "Direct measurement of sheath electric field distribution in front of substrate in electron cyclotron resonance plasma by laser-induced fluorescence technique". *Japanese Journal Applied Physics,* Vol. 39, pp.L116-L118.
9.Takiyama, K., Oda, T. and Sato, K. (2001): "Spectroscopic measurement of biasing effect on sheath electric field distribution in front of a metal plate inserted in plasma flow". *Journal of Nuclear Materials,* Vol.290-293, PP.976-979.
10.Yeh, F. B. and Wei, P. S. (2005): "The effect of sheath on plasma momentum transport to an electrically biased surface". *International Journal of Heat and Mass Transfer,* Vol. 48, pp.2198-2208.